Journal of Scientific Research & Reports
3(11): 1465-1474, 2014; Article no. JSRR.2014.11.004

SCIENCEDOMAIN *international*
www.sciencedomain.org

Enhancing AC Electrothermal Micropumping by Integrating Temperature Bias and Surface Modification

Nazmul Islam[1*]

[1]*Director MEMS/NEMS Research Lab School of Engineering and Computational Sciences, The University of Texas at Brownsville, Brownsville, TX 78520, United States.*

Author's contribution

This whole work was carried out by the author NI.

Short Research Article

Received 31st December 2013
Accepted 8th April 2014
Published 21st April 2014

ABSTRACT

This paper describes an experimental study of the improvement of bi-directional AC (Alternating Current) electrothermal micropump velocity by a surface modification process and the addition of a temperature bias. The work focuses on exploiting external temperature bias to enhance micropumping by AC electrothermal (ACET) effect. Adding temperature bias to a symmetrical electrode setup provides an advantage of bi-directional characteristic. Here an integrated AC micropump design is proposed, which is expected to solve the problem of on-chip pumping for biofluids. A polymer base nanocomposite coating consisting of a homogeneous mixture of silicon nanoparticles in polydimithylsiloxane (PDMS) is used to improve the hydrophobicity of the micropump surfaces. Due to the hydrophobic nature of PDMS and the monolayer coating with nanoscale surface roughness, the hydrophilic surface of temperature biased ACET micropump will transform to a hydrophobic surface. In addition to hydrophobicity improvement, adding a thin nanocomposite monolayer will physically separate the electrodes from the pumping liquid, thus eliminating their reaction, which is usually observed due to the application of voltage. In addition, the surface modification of micropump will decrease the friction loss and improve the pumping velocity. All experiments were done at 100 kHz V_{AC} that also suppress the bubble generation. As a result, we could apply 7.5 Vrms (equivalent to 21.2 V, peak to peak) voltages to the symmetrical electrode arrays and higher pumping rates (2100 microns/sec) are achieved.

**Corresponding author: E-mail: nazmul.islam@utb.edu;*

Keywords: AC electrothermal; micropump, symmetrical electrode; biomedical; hydrophobic coating; nanocomposite monolayer; surface modification.

1. INTRODUCTION

Micropumps are primarily designed to transport a small amount of fluid for a wide range of microfluidic applications, e.g., drug delivery, bio-fluid analysis, and microelectronics cooling. Micropumps are developed based on mechanical and non-mechanical driving methods to control the flow of different fluids in various devices and sensors for specific applications. Non-mechanical pumps have several advantages over mechanical pumps [1,2], such as higher reliability (for no moving parts), easy implementation into microfluidic devices, and continuous pumping of fluids. Some techniques of non-mechanical pumping method utilizes Electroosmosis (EO) or Electrothermal (ET) to transport fluids through microchannels.

In microscale, mechanical micropumps encounter very high flow resistance due to high friction coefficient which imposes stringent requirement on the strength of fluid channels and interconnects. Furthermore, because of large surface to volume ratios in microchannels, surface tension and viscous forces play an important role in deciding the flow characteristics inside the microchannels [3-4]. For this reason, application of electrokinetic micropumping has dominated the microscale transport of fluids in microfluidic devices. A significant driving force underlying this research has been the integration of pumping mechanisms in micro total analysis and biomedical devices [5]. Since the electrokinetic micropumps involve no moving parts, they are easy to fabricate, unsusceptible to particulate contamination, and compatible with microchannel integration. It is worth mentioning that direct current (DC) electrokinetic micropumps have already been integrated into several fluidic analysis systems [6-8]. However, DC electrokinetic micropumps have severe weaknesses, such as high voltage requirement in KV range (i.e., difficult to integrate them into microsystems), bubble generation, and electrode reactions [9]. Newly emerged alternating current (AC) electrokinetic micropumps can avoid the aforementioned disadvantages [10]. AC electrothermal (ACET) involves electric, thermal, and fluidic phenomena simultaneously. Loire et al. [11], Kumar et al. [12-13] and Williams et al. [14] present the demonstrations of ACET manipulation and pumping of biofluids. These papers experimentally validated the work on ACET modelling at high voltage and high conductivity. In this paper the ACET pump is realized by applying AC electric signals over interdigitated microelectrodes. Our proposed temperature biased ACET micropump combines the temperature biasing and AC signals with the electrothermal technique to control the fluid flow at the surface of microchannels. The resulting micropump is capable of producing bi-directional flow (unlike many existing micropumps) and is highly controllable. This micropump is expected to operate with high frequency AC voltage and can be easily fabricated and integrated with MEMS devices using the existing microfabrication techniques. This ACET micropump is well suited to efficiently pump biofluid, which generally have high conductivity and cannot be well manipulated by other AC electrokinetic forces [15]. ACET force directly applied to the bulk fluid and ACET models pick up non-slip condition for the electrode surface. Additionally, the magnitude of ACET velocity does not merely depend on the field strength, but also the temperature gradient, which could reach its maximum at some distance from the electrodes [9]. Therefore ACET flow maximum is within the bulk.

The above property of velocity profile has an impact on the performance of electrokinetic devices at a very small scale. ACET velocity has little dependency on frequency when it is well below the cross-over frequency. Coulomb force will dominate at low frequency. For aqueous solutions with temperature around 298K, the conductivity and permittivity change

with the temperature gradient. The cross-over frequency of ACET force shows the transition frequency of 170 MHz for a solution with conductivity of 0.224 S/m [16]. Such result indicates that ACET fluid flow is the result of Coulomb force under usual experimental conditions.

AC electrothermal (ACET) flow is a well-known phenomenon, which arises in systems with nonuniform permittivity and conductivity. In such a system, a local free charge distribution is present. The local charge density responds to the applied electric field resulting in a non zero volume force on the fluid. Electrothermal effect arises from uneven Joule heating due to an electric current flowing through the fluid. The theoretical foundation of ACET mechanism is a coupling problem which involves electric, thermal and fluidic mechanical formulations. At the time an ac signal is applied, the electric field is established within the solution. Charged particles are attracted by the electrode with opposite polarity and migrate, which forms the ionic current. The current density in the fluid is expressed as:

$$J = \sigma E = (\mu_+ + \mu_-)\, c\, E \tag{1}$$

Where σ is the fluid conductivity, E is the applied electric field, c is the concentration, μ_+ and μ_- is the limiting ion conductivity for anions and cations which are constants at 298K. The equation (i) indicates the resistive manner of fluid bulk. In addition, the electrical Reynolds number is much less than one in microfluidic systems, implying that ohmic current dominates.

2. AC ELECTROTHERMAL WITH TEMPERTURE BIAS

ACET effect refers to fluid motion induced by temperature gradients in the fluid in the presence of AC electric fields [7]. When an electric field E is applied over the fluid with electrical conductivity σ, Joule heating of the fluid will take place according to the energy balance equation:

$$k\nabla^2 T + \frac{1}{2}\langle \sigma E^2 \rangle = 0 \tag{2}$$

Where T is temperature and k is the thermal conductivity. For our microsystem, heat convection is small compared to heat diffusion [16-18]. So here the temperature equation assumes the simplified form with Joule heating as the energy source. If the field strength E is non-uniform, there will be spatial variation in heat generation, which leads to temperature gradients ∇T in the fluid. Generally, the change of fluid conductivity and permittivity heats the solution. The temperature gradients increase linearly with conductivity and so enhance the ACET flow. Such variations cause the generation of free charges which intends to move under Coulomb force and drag the fluid [16]. The heating process can be either from the fluid Joule heating, or externally applied temperature source, or light source (e.g. light illumination) [14].

At high conductivity and high voltage, the Joule heating in the fluid is significant which leads to an AC electrothermal fluid flow. The frequency is chosen high enough to prevent bubble generation. The net pumping motion by ACET effect was observed using symmetric interdigitated planar electrodes (Fig. 1). When using symmetric electrode pattern, the direction of fluid can be changed by changing the temperature biasing on the electrode array. Bi-directional fluid velocity can be obtained by changing the temperature biasing. As this is a symmetrical electrode pattern, the pumping direction can be changed by changing the hot and cold electrode lead. Now we have a direction of fluid flow from right to left (Fig.

4) for higher temperature in the right electrode. As soon as we change the temperature field, the fluid will flow from left to right.

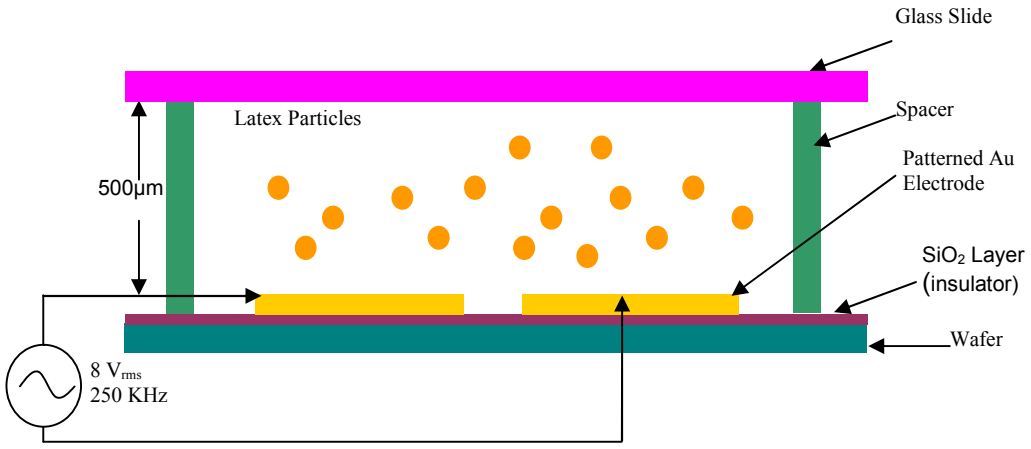

Fig. 1. Schematic of the experimental setup of Symmetric Electrode configuration of ACET micropump. External temperature is applied in the experimental setup by using a temperature controlled soldering iron. Temperature bias is the principal reason of fluid flow in this symmetric electrode array configuration. In our experiment we applied the temperature in the right electrodes of the array

The working fluid was seeded with latex micro-particles to track fluid motion. At the beginning of experiments, the micro-particles were located at one end of the chamber. After applying the electric field, they quickly moved forward and occupied the whole channel, showing a successful pumping attempt by ACET effect. The micropumping prove the abilities of ACET effect in fluid handling and offers its use for further study in lab-on-a-chip (LOC) devices.

In our experimental study of ACET velocity, the applied voltage was varied for a fixed heat flux of 10^4 W/m^2 and fixed fluid conductivity of 1 S/m. In this section, heat flux and fluid conductivity are varied in the experimentation to study their effects on ACET velocity, while the applied AC voltage is fixed at 8 V_{rms} to simplify the discussion. The ACET pump consists of an array of interdigitated electrodes of 100 nm thick coating on an oxidized silicon substrate. The symmetric electrodes are 80 μm wide electrodes with 40 μm gap between them and gap between pairs of electrodes is 100 μm. A 100 μm high microchannel of PDMS (polydimethylsiloxane) is sealed over the electrodes. The silicon sample was prepared using a standard cleanroom microfabication process. Au/Cr (90nm/10nm thickness) electrodes were fabricated by lift-off procedure in IC processing. Cr is the adhesion layer between the substrate and Au, and Au is in contact with electrolytes. The pattern was transferred from the mask to the Si wafer by standard photolithographic technique. The patterned electrodes are then fabricated by electron beam evaporation and lift-off process. The electrodes were 8 mm long, 0.1 μm (100 nm) thick, 80 μm wide with a 40 μm in-pair separation and 100 μm between-pair gap separation. A PDMS microchannel of 100-μm depth was peeled off from the mold to fabricate the microfludic chamber. Particles with sizes of 200 nm (fluorescent, Molecular Probes) and 1 μm (Polystyrene spheres; Fluka Chemica) were suspended in high conductive water to track fluid motion.

3. SURFACE MODIFICATION USING HYDROPHOBIC MONOLAYERS

A hydrophobic surface is a surface that can be described as “water repellant” with many applications. Due to the non-polarity of the hydrophobic surface, polar molecules such as water tend to resist any form of attraction/adhesion to the solid surface. In this research, hydrophobic thin film polymer coatings were developed using polydimethylsiloxane (PDMS) compounds as a base material. To further improve the hydrophobicity, surface textures/roughness was created on PDMS in micro and nano scales by inclusion of silicon nanoparticles (Si-NP). The silicon nanoparticles are non-toxic (in contrast to other nanomaterials), semiconductor, and stable fluorescence at different wavelengths. They are easily synthesized, can be dispersed in various types of solvents, and are compatible with PDMS [19,20]. Uniform thin layers of plain PDMS and polymeric nanocomposites (combination of solvent, nanoparticles and PDMS) were spin coated on flat solid substrates and their hydrophobicity was examined using a contact angle measurement device. The implementation of this research has a wide range of applications such as in drug delivery, bio-fluid analysis, microfluidics and multifunctional biocompatible material. In another attempt, flat solid surfaces with pre-existing surface roughness/textures (e.g., silicon wafers with etched arrays of regularly spaced circular holes in micron sizes and sand papers with various grit sizes) were used as molds to create very fine surface roughness/textures and then their effects on hydrophobicity characteristics of PDMS was investigated. Promising results were obtained and more comprehensive studies will be conducted as our future work. For hydrophobic nature of PDMS and the resulting surface texture/roughness (created by nanoparticles or textured solid molds) the hydrophilic surfaces can be transformed into surfaces with hydrophobic characteristics. Uncured PDMS is often diluted with various types of solvents in different ratios to spin thin films (<5 μm) on solid surfaces. In this work for the nanocomposite coating, 0.2 wt% of Si-NP, as an optimum concentration ratio, with average size of ~20-30 nm was dispersed in tert-butyl alcohol (TBA), Hexane and Tolune, among which, TBA resulted the best uniform distribution. Therefore, TBA was used for uniform dispersion of Si-NP and dilution of PDMS for fabrication of thin hydrophobic monolayers. For the dispersion, Si-NP/TBA was first sonicated for 30 min in a caped glass container in a 45ºC (Celsius unit) heated bath and then stirred using a magnetic stirrer hotplate at 45 °C for ~3 hours. Next, 1 part (wt%) of PDMS base was added to 4 parts (wt%) of Si-NP/TBA mixture in the same closed container and then stirred again on the hotplate at 45ºC for ~5 hours. Once the uniformity of nanoparticles dispersion was confirmed (using a high magnification optical microscope), 0.1 part (wt%) of PDMS hardener was added to the mixture and then carefully stirred for uniform mixing. The mixture was degassed for 3-4 minutes in a sonicator and then spin-coated over the surface of glass slides at ~6000 rpm for 4-6 minutes. Finally, the coated glass slides were placed on a 60ºC hotplate until fully cured (1–2 hours). Later, the same nanocomposite mixture was used to coat our micropump surfaces and fabricate micro-channels to improve the pumping efficiency.

It should be mentioned that during the mixing process and prior to spin coating, the mixture was always confined in a closed cap glass container and the majority of TBA solvent was remained in the mixture maintaining a very low viscosity and facilitating very thin film depositions (Fig. 2a). However, it was observed that nanoparticles tend to agglomerate during the high-velocity spinning process (Fig. 2c-2e), due to rapid evaporation of TBA solvent from the mixture. Alternatively, a new batch of PDMS base Si-NP nanocomposite coating was processed following the same procedure, as explained above, except that the TBA solvent was allowed to slowly evaporate prior to spin coating (shown in Fig. 2b). As one would expect, the new spin-coated thin films were somewhat thicker than those obtained

from former method. In return, the optical microscopy examination of the new thin film nanocomposites showed negligible nanoparticle agglomerations suggesting that Si-NPs are uniformly distributed in the PDMS (shown in Fig. 2f) creating very fine and uniform surface textures/roughness.

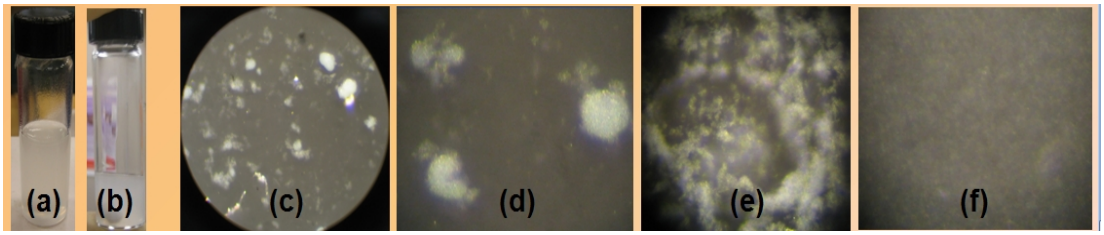

Fig. 2. (a) Low viscosity and (b) viscous nanocomposite mixture. (c) Low, (d) medium, and (e) high magnification optical micrographs of nanoparticles agglomeration in low viscosity nanocomposite thin films. (f) Optical micrograph of uniform dispersion of nanoparticles in viscous nanocomposite thin film

The hydrophobicity was measured by examining water contact angle on thin film coatings. The interaction of liquid droplet with flexible Si-NP/PDMS nanocomposite monolayers was analyzed on flat substrates. Liquid droplet static contact angle was measured using a contact angle measurement device for samples with or without coatings (see Fig. 3). To get a quantitative measure for the hydrophobicity, two methods were used. The first method was the direct reading of contact angle by adjusting the angle meter gauge on the angle meter screen. The second method was calculation of contact angle employing the Eq. (3), i.e., Tantec's Half Angle Formula, and using the measured values of the height and the width of water droplets.

$$\theta = \tan^{-1}\left(\frac{H}{R}\right) \tag{3}$$

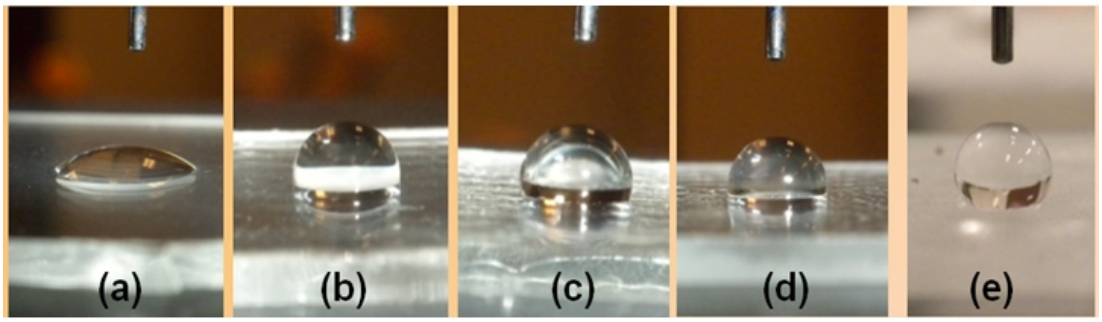

Fig. 3. Water droplets on flat glass substrates with (a) no coating, (b) plain PDMS coating, (c) TBA diluted low viscosity Si-NP/PDMS nanocomposite coating, (d) viscous Si-NP/PDMS nanocomposite coating and (e) PDMS coating with a very fine surface texture/roughness

In the above formula, θ is the contact angle, H is height of the water droplet and R is radius of the base. Table 1 shows the results (averaged values of at least five readings) obtained from contact angle measurement for bare and coated glass slides. The standard deviations

for the contact angle results were less than 1.6° for all the measurements. It should be mentioned that the contact angle values that are obtained from direct reading technique is a result of one single reading while the contact angle values from second techniques are calculated based on two readings (i.e., droplet height and radius). Considering a constant error for every reading (i.e., contact angle, droplet height, and droplet radius) on the angle meter screen, due to inaccuracy in reading of the values, it is believed that the results obtained from the first technique are more accurate.

Table 1. Contact angle measurement results for glass slides with and without PDMS or Si-NP/PDMS nanocomposite monolayer coatings

Coating type	None	Plain PDMS	Low viscosity Si-NP/PDMS nanocomposites	Viscous Si-NP/PDMS nanocomposite
Droplet volume (mL)	0.005	0.005	0.005	0.005
Droplet height (Grits)	4	8	8.75	8.90
Droplet radius (Grits)	10.50	7.13	7.17	7.10
Contact angle (direct reading)	43º	98.75º	103º	104.25º
Contact angle (from Eq. (1))	41.7º	96.40º	101.34º	102.84º

A considerable increase in contact angle was measured due to the presence of Si-NP/PDMS nanocomposite monolayer coating on the glass slide surfaces. Because of the hydrophobic characteristics of these modified solid surfaces, the friction loss is decreased and eventually the pumping velocity can be improved in micropump devices.

4. RESULTS AND DISCUSSION

ACET flow is examined using microfabricated arrays of symmetric electrode pairs on silicon substrate. Particles with sizes of 200 nm and 1 μm were suspended in high conductive water to track fluid motion (Fig. 4). A frequency range from 100 kHz to 500 kHz was determined to be optimal for observing particle motion in the high conductive (0.25 S/m) fluid suspension. The particle movement was observed using confocal microscope through the top of PDMS microchamber. The average fluid velocity was determined by recording the time it took the particles to travel a known distance. The traveled distance and time were determined from video taken with a Moticam Digital 3.0 MP camera. The focal plane of microscope was ~30 μm above the wafer surface.

Thermal biasing was realized by using temperature variable soldering iron to connect with the two bonding pads of electrodes. The bonding pads are 6 mm wide and 8 mm long, and are located 2 mm away from the microelectrode array. Soldering iron was set to 150ºC. Where the soldering iron contacted the bonding pads were measured to be at 35ºC (Room temperature was 22ºC). The temperature difference between the electrodes inside the microchannel was expected to be much less than that at the bonding pads due to heat transfer from the electrodes to the silicon substrate and ambience.

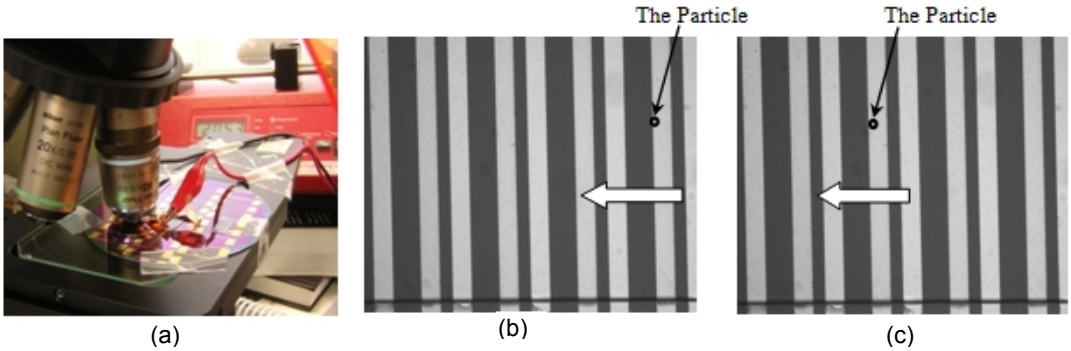

Fig. 4. (a) Experimental setup for the ACET micro-pump with temperature bias. (b) and (c) Image sequence of a particle advancing through the array of electrodes, at t=0 (b) and t=1.5 sec (c). Due to the application of AC voltage with Temperature to symmetric electrode arrays net micropumping was achieved

The experimental results shown in Fig. 5 illustrate the capabilities of ACET effect as a candidate for conductive bio-fluid manipulation. Image sequence was recorded for a particle cluster advancing though electrode pairs when an AC signal of 2.5 Vrms to 7.5 Vrms at 250 kHz was applied. The magnitude of other forces (ACEO, DEP, buoyancy, Brownian motion and gravity) were quantitatively compared as a possible to induce fluid flow in this operating condition. They are all ruled out because of negligible influence to the observed flow, leaving ACET to be the only responsible mechanism for micropumping. Considerable flow velocities at the order of hundred microns per second were recorded in our experiments at low voltages (<8 Vrms).

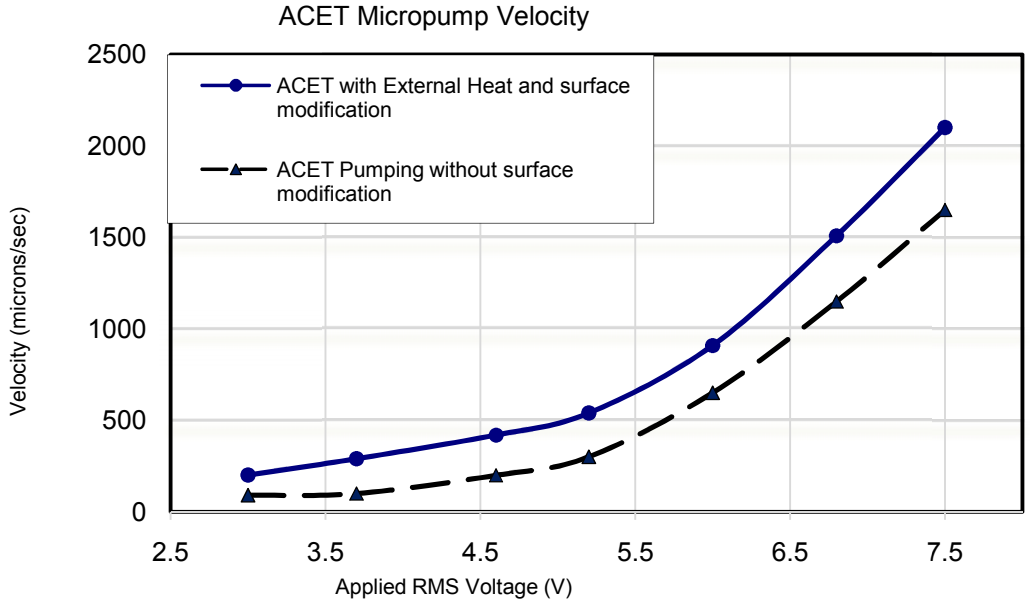

Fig. 5. ACET Micropump velocity as function of applied RMS voltage. Micropump velocity is calculated by measuring the tracer particle velocity under the microscope

With temperature biasing, ACET flows always went from the hotter electrodes towards the other electrodes. For the result, the external heating element produces the flow velocity that varies up to ~1500 micron/sec for temperature gradient. Fig. 5 also compares the micropumping velocities for two different surface characteristics. For each applied voltage, four data points were averaged to calculate the particle velocities. Our calculated error for each data point was less than 2%. The velocity of micropump increases after adding the Si-NP/PDMS nanocomposite monolayer. In this case the hydrophobic surface will improve the lossy effect on surface. Again, the hydrophobic surface reduces the reaction sensitivity as there is no direct contact between the solvent and electrodes. Therefore, we can apply higher voltages and increase the micropumping velocity. The highest velocity measurement was 2100 μm/sec, which is much higher than the velocity of the micropump without a hydrophobic monolayer coating. The trade-off between the surface characteristic and electric field strength will be a focus of our future investigation. In addition, the presence of the hydrophobic coating does eliminate the electrode reaction with working fluid and much higher voltages can be applied, leading to higher micropump velocities.

5. CONCLUSION

This paper is devoted to the investigation of hydrophobic surface modification effects on optimization of ACET micropump by integrating temperature biasing. The experimental flow measurements were performed on symmetric electrode array micropump configurations manufactured using standard micro-fabrication technologies. The experimental results confirm that using a symmetric electrode array excited by temperature bias leads to a significant improvement in flow rates. Various techniques have been used to create hydrophobic coatings for surface modification of the micropump components to reduce the friction losses and achieve higher pumping velocities. Furthermore, it was observed that the addition of Si-NP/PDMS nanocomposites hydrophobic monolayer eliminates the electrode reaction with working fluids. As a result, higher AC voltages were applied and thus, higher pumping velocities can be achieved. Our future work will focus on control unit of the micropump by utilizing the micropump velocity and applied current as input signals. This can easily be realized by integrating an electronic feedback control circuit with temperature controlled ACET micropump. Improved performance of ACET devices is expected with optimized design. The advance with ACET devices will greatly expand the application scope of electrokinetics in bio-sample manipulation or biochemical analysis in micro/bio-fluidic chips.

COMPETING INTERESTS

The author has declared that no competing interests exist.

REFERENCES

1. Loucaides N, Ramos A, Georghiou G. Novel systems for configurable AC electroosmotic pumping. J Microfluid & Nanofluid. 2007;3:709-714.
2. Liu S, Pu Q, Lu JJ. Electric field-decoupled electroosmotic pump for microfluidic devices. Journal of Chromatography A. 2003;1013:57-64.
3. Green NG, Ramos A, Gonzalez A, Morgan H, Castellanos A. Fluid flow induced by nonuniform ac electric fields in electrolytes on microelectrodes. I experimental measurements. Phys Rev E. 2000;61:4011–18.

4. Ramos A, Gonzalez A, Castellanos A, Green NG, Morgan H. Pumping of liquids with ac voltages applied to asymmetric pairs of microelectrodes. Phys Rev E. 2003;67:056302.
5. Iverson BD, Garimella SV. Recent advances in microscale pumping technologies: A review and evaluation. J Microfluid & Nanofluid. 2008;5(2):145–174.
6. Koschwanez JH, Carlson RH, Meldrum DR. Thin PDMS Films Using Long Spin Times or Tert-Butyl Alcohol as a Solvent. PLoS One. 2009;4(2):45-72.
7. Chen CH, Santiago JG. A Planar Electroosmotic Micropump. Journal of Microelectromechanical Systems. 2002;11:6.
8. Islam N, Askari D. Optimizing biased AC Electroosmosis Micropump by Hydrophobic Nanoparticle Monlayer. Proceedings ASME International Mechanical Engineering Congress and Exposition, Vancouver. 2010;851-854.
9. Lian M, Islam N, Wu J. AC Electrothermal Manipulation of Conductive Fluids and Particles for Lab-chip Applications. IET Nanobiotechnology. 2007;1(3):36-43.
10. Studer V, Pepin A, Chen Y, Ajdari A. An integrated AC electrokinetic pump in a microfluidic loop for fast and tunable flow control. Analyst. 2004;129:944–949.
11. Loire S, Kauffmann P, Mezic I, Meinhart CD. A theoretical and experimental study of ac electrothermal flows. J Phys D Appl Phys. 2012;45:185-301.
12. Kumar A, Williams SJ, Chuang H-S, Green NG, Wereley ST. Hybrid opto-electric manipulation in microfluidics – opportunities and challenges. Lab on a Chip. 2011;11:2135–2148.
13. Kumar A, Cierpka C, Williams SJ, Kahler CJ, Wereley ST. 3D3C velocimetry measurements of an electrothermal microvortex using wavefront deformation PTV and a single camera. J Microfluid & Nanofluid. 2011;10:355–365.
14. Williams SJ. Enhanced electrothermal pumping with thin film resistive heaters. Electrophoresis. 2013;34:1400-1406.
15. Askari D, Islam N. Improving the Pumping Efficiency of a Micropump Using Hydrophobic Nanocomposite Coating. Proc. ASME 45240, 8: Mechanics of Solids, Structures and Fluids. 2012;275. DOI: 10.1115/IMECE2012-87837.
16. Wu J, Lian M, Yang K. Micropumping of Biofluids by AC Electrothermal Effects. Appl Phys Letter. 2007;90:234103.
17. Lian M, Wu J. Ultra Fast Micropumping by Biased AC Electrokinetics. Appl Phys Lett. 2009;94(6):064101.
18. Lian M, Wu J. Microfluidic flow reversal at low frequency by AC electrothermal effect. J Microfluid & Nanofluid. 2009;7:757-765.
19. Islam N, Lian M, Wu J. Enhancing Cantilever Capability with Integrated AC Electrokinetic Trapping Mechanism. J Microfluid & Nanofluid. 2007;3(3):369-375.
20. Singh MP, Atkins TM, Muthuswamy E, Kamali S, Tu C, Louie AY, Kauzlarich SM. Development of Iron-Doped Silicon Nanoparticles As Bimodal Imaging Agents. ACS Nano. 2012;6(6):5596–5604.

Peer-review history:
The peer review history for this paper can be accessed here:
http://www.sciencedomain.org/review-history.php?iid=493&id=22&aid=4370